ISSN: 2639-0108

Research Article

Advances in Theoretical & Computational Physics

Generation of the GHZ and the W State in a Series of Rydberg Atoms Trapped in Optical Lattices

Aneesh Ramaswamy[1], Albert F. Latypov[2], and Svetlana A. Malinovskaya[1*]

[1]*Department of Physics, Stevens Institute of Technology, Hoboken, NJ 07030 USA*

[2]*Institute of Theoretical an Applied Mechanics, Siberian Division, Russian Academy of Sciences, Novosibirsk, 630090 Russia*

[*]Corresponding author
Svetlana A. Malinovskaya, Department of Physics, Stevens Institute of Technology, Hoboken, NJ 07030 USA.

Submitted: 14 Jun 2022; **Accepted:** 22 Jun 2022; **Published:** 05 Jul 2022

Citation: *Ramaswamy. A., Latypov. A.F., and Malinovskaya. S.A. (2022). Generation of the GHZ and the W State in a Series of Rydberg Atoms Trapped in Optical Lattices. Adv Theo Comp Phy, 5(3), 476-484.*

Abstract

In this work, we present a quantum control methodology to create multi-particle entangled states of two typical classes, the W and the Greenberger-Horne-Zeilinger (GHZ). The methodology is demonstrated on a generation of the W and GHZ three-atomic states via the mechanism of two-photon passage using overlapping chirped pulses and the interplay of the chirp rate, the one-photon and two-photon detuning, the peak Rabi frequency and the strength of the Rydberg-Rydberg interactions. A chain of N alkali ^{87}Rb atoms in an optical lattice interacting with two laser fields is modeled within a semi-classical theory. The strategy to create different classes of multi-particle entangled states was revealed through performed dressed state analysis.

1. Introduction

Ultracold physics with atoms in optical lattices opened up abundant opportunities for studies of quantum many-body phenomena due to a tunable structure of the optical potentials. Atoms placed in such potential and excited to the Rydberg states interact through the long-range interactions, which are of dipole-dipole or the van der Waals type depending on the interatomic distance. Modern control techniques permit manipulations of collective excitations of trapped atoms to Rydberg states aiming at a generation of different types of entangled states - the workhorse of quantum enabled tasks. Here, we present a robust quantum control methodology to selectively excite collective states in systems of few atoms leading to a generation of different types of entangled states within collective spin systems involving Rydberg atoms.

There are three major classes of multiparticle entangled states: the GHZ states, the W states, and the cluster states [1-3]. Notably, these classes of states are non-separable and cannot be transformed into each other by local quantum operations [4]. The GHZ state represents a maximally entangled state, while the W state is unique in that a single-particle measurement of the state only collapses it by one order. GHZ states are best utilized as quantum channels for teleportation, while W states are necessary for secure quantum communication [5, 6]. In order to take advantage of the properties of multiparticle entangled states, it is important to be able to generate these states on demand. There has been a significant effort regarding preparation of the GHZ and the W states using various platforms, from atomic systems to quantum dots to superconducting qubits [7-9].

In this paper, the present a method for a preparation of the GHZ and the W multiparticle entangled states for an arbitrary number of atoms having the energy gaps in the many-body spectrum greater than the τ^{-1}, where τ is the chirped pulse duration. We demonstrate a high-fidelity of these states' generation and a fast time scale.

The methodology to generate entangled states is based on using circularly polarized and linearly chirped μs laser pulses and carefully chosen field parameters, namely the peak Rabi frequency, the chirp rate and the detuning. A generation of the desired states is expected to be robust. Thus, we were seeking an adiabatic passage type of solutions. The roots to these solutions may be revealed through the dressed state analysis, which also suggests the limitations of adiabatic regime for certain types of entanglement.

We use a model system of a chain of alkali ^{87}Rb atoms in an optical lattice, where each atom is considered as a system of effective spin states, arranged in the three-level ladder configuration having the ground spin state $|g\rangle$, the intermediate spin state $|e\rangle$, and the excited Rydberg spin state $|r\rangle$, shown in Figure 1. The GHZ state is known to be a superposition state of all atoms in the ground state and all atoms in the excited, e.g., Rydberg state. For a triatomic configuration, the GHZ state reads

$$|GHZ\rangle = \frac{|rrr\rangle + |ggg\rangle}{\sqrt{2}}. \quad (1)$$

The W state is a quantum superposition of all possible pure states in which one atom is in, e.g., the ground state, while all others are in the Rydberg state. A triatomic W state reads

$$|W\rangle = \frac{|grr\rangle + |rgr\rangle + |rrg\rangle}{\sqrt{3}}. \quad (2)$$

The energy of the GHZ and the W states depends on the interaction strength between atoms, V_{ij}, which is a function of the distance between atoms r_{ij} in an optical lattice. In the one-dimensional case, the van der Waals interaction is given as

$$V_{ij} = C/r_{ij}^6 = C/(s/(n-1))^6. \quad (3)$$

Here, C is the van der Waals interaction constant, s is the length of the optical lattice, and n is the number of minima or, equivalently, the number of atoms. Due to the fact that V_{ij} is dependent on the positions of the atoms, it can be changed by manipulating the optical lattice. For a given V_{ij}, we control the dynamics of a two-photon excitation of the chain of atoms by laser pulses, prepared based on the developed control schemes to produce transitions, that stir the multiparticle system into the desired entangled state.

We justify the developed control schemes for the GHZ and the W states by demonstrating their generation in the framework of the exact time-dependent Schrödinger solution and a calculation of the fidelity of each state formation. The paper is arranged as follows. In Sections II and III, we derive the single-particle and the multiparticle Hamiltonian in the field-interaction representation; in Section IV, we discuss the quantum control methodology on an example of a three-atomic chain, demonstrate its deduction from an effective two-level approximation and introduce the entanglement fidelity for the GHZ and the W state; Section V is devoted to a numerical verification of the control mechanisms of the creation of the GHZ and the W states via fidelity as a function of the chirp rate and the peak Rabi frequency; Section VI summarizes findings.

II. The Hamiltonian and the Equation of Motion for a Single Atom

We derive the Hamiltonian that describes the interaction of atoms with the laser field by first deriving the Hamiltonian of a single three-level atom and working up to the entangled triatomic state.

For an atom modeled by a three-level ladder system, shown in Figure 1, the field interaction Hamiltonian H describing the interaction of the atom with two external fields reads

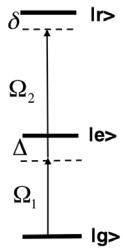

Figure 1: A schematic of a three-level atom where $|g\rangle$ is the ground state energy, $|e\rangle$ is the intermediate state energy, $|r\rangle$ is the excited state energy, the $\Omega_1(t)$ is the pump Rabi frequency and the $\Omega_2(t)$ is the Stokes Rabi frequency, and the frequencies are time-dependent in a general case.

$$H = \frac{\hbar}{2}\begin{bmatrix} \omega_g & \Omega_1(t) & 0 \\ \Omega_1(t) & \omega_e & \Omega_2(t) \\ 0 & \Omega_2(t) & \omega_r \end{bmatrix}. \quad (4)$$

Here $\Omega_1(t) = \frac{-\mu_{eg}E_1(t)}{\hbar}$ and $\Omega_2(t) = \frac{-\mu_{re}E_2(t)}{\hbar}$ are the Rabi frequencies, and $E_1(t)$ and $E_2(t)$ are the laser pulses that couple the ground to the intermediate state, $|g\rangle \rightarrow |e\rangle$, and the intermediate to the excited state, $|e\rangle \rightarrow |r\rangle$, respectively; μ_{ij} is the transition dipole moment matrix element on a respective transition. These fields are linearly chirped and can be written as

$$\begin{aligned} E_1(t) &= \frac{E_{10}(t)}{2}(e^{i\omega_p t + \frac{i\alpha_1 t^2}{2}} + e^{-i\omega_p t - \frac{i\alpha_1 t^2}{2}}) \\ E_2(t) &= \frac{E_{20}(t)}{2}(e^{i\omega_s t + \frac{i\alpha_2 t^2}{2}} + e^{-i\omega_s t - \frac{i\alpha_2 t^2}{2}}), \end{aligned} \quad (5)$$

where α_1 and α_2 are linear chirp parameters, ω_p and ω_s are the applied pump and Stokes fields frequency. These frequencies are best defined by their relation to the one-photon detuning Δ and the two-photon detuning δ:

$$\Delta = \omega_e - \omega_p, \delta = \omega_r - (\omega_p + \omega_s). \quad (6)$$

We define the wave function of the three-level ladder system in the Dirac notation as $|\Psi(t)\rangle = A_g(t)|g\rangle + A_e(t)|e\rangle + A_r(t)|r\rangle$, where $A_g(t)$, $A_e(t)$ and $A_r(t)$ are the probability amplitudes for the ground, the intermediate, and the excited state respectively in the Schrödinger representation. The Schrödinger equation for this system using the Hamiltonian in Eq. (4) reads

$$i\hbar\begin{bmatrix} \dot{A}_g(t) \\ \dot{A}_e(t) \\ \dot{A}_r(t) \end{bmatrix} = \frac{\hbar}{2}\begin{bmatrix} \omega_g & \Omega_1(t) & 0 \\ \Omega_1(t) & \omega_e & \Omega_2(t) \\ 0 & \Omega_2(t) & \omega_r \end{bmatrix}\begin{bmatrix} A_g(t) \\ A_e(t) \\ A_r(t) \end{bmatrix}. \quad (7)$$

Expanding the Schrödinger Equation (7), we obtain the differential equations for probability amplitudes to see the evolution of the ladder system in the Schrödinger representation:

$$\begin{aligned} i\dot{A}_g(t) &= \frac{w_g}{2}A_g + \frac{\Omega_{10}(t)}{2}(e^{i\omega_p t + \frac{i\alpha_1 t^2}{2}} + e^{-i\omega_p t - \frac{i\alpha_1 t^2}{2}})A_e \\ i\dot{A}_e(t) &= \frac{\Omega_{10}(t)}{2}(e^{i\omega_p t + \frac{i\alpha_1 t^2}{2}} + e^{-i\omega_p t - \frac{i\alpha_1 t^2}{2}})A_g + \\ &\quad \frac{\omega_e}{2}A_e + \frac{\Omega_{20}(t)}{2}(e^{i\omega_s t + \frac{i\alpha_2 t^2}{2}} + e^{-i\omega_s t - \frac{i\alpha_2 t^2}{2}})A_r \\ i\dot{A}_r(t) &= \frac{\Omega_{20}(t)}{2}(e^{i\omega_s t + \frac{i\alpha_2 t^2}{2}} + e^{-i\omega_s t - \frac{i\alpha_2 t^2}{2}})A_e + \frac{w_r}{2}A_r. \end{aligned} \quad (8)$$

In order to make probability amplitudes time independent in the absence of the external fields, we move the system into the frame rotating with the fields by defining

$$\begin{aligned} A_g(t) &= a_g(t) \\ A_e(t) &= a_e(t)e^{-i\omega_p t - \frac{i\alpha_1 t^2}{2}} \\ A_r(t) &= a_r(t)e^{-i\omega_p t - \frac{i\alpha_1 t^2}{2} - i\omega_s t - \frac{i\alpha_2 t^2}{2}}, \end{aligned} \quad (9)$$

where $a_g(t)$, $a_e(t)$ and $a_r(t)$ are the time-dependent probability amplitudes of the ground, the intermediate, and the excited state respectively in the field interaction representation. This change of

representations aids in revealing the mechanisms of light-matter interaction and the quantum control strategy.

By substituting Equation (9) into Equation (8), taking derivatives and applying the rotating wave approximation we arrive at

$$\begin{aligned} i\dot{a}_g &= \frac{w_g}{2}a_g + \frac{\Omega_{10}(t)}{2}a_e \\ i\dot{a}_e &= \frac{\Omega_{10}(t)}{2}a_g + \frac{1}{2}(w_e - w_p - \alpha_1 t)a_e + \frac{\Omega_{20}(t)}{2}a_r \\ i\dot{a}_r &= \frac{\Omega_{20}(t)}{2}a_e + \frac{1}{2}(w_r - w_p - \alpha_1 t - w_s - \alpha_2 t)a_r. \end{aligned} \tag{10}$$

Applying Equation (6) simplifies further this set of differential equations

$$\begin{aligned} i\dot{a}_g &= \frac{w_g}{2}a_g + \frac{\Omega_{10}(t)}{2}a_e \\ i\dot{a}_e &= \frac{\Omega_{10}(t)}{2}a_g + \frac{1}{2}(\Delta - \alpha_1 t)a_e + \frac{\Omega_{20}(t)}{2}a_r \\ i\dot{a}_r &= \frac{\Omega_{20}(t)}{2}a_e + \frac{1}{2}(\delta - (\alpha_1 + \alpha_2)t)a_r. \end{aligned} \tag{11}$$

We can insert one additional simplification by stating the ground state energy $\omega_g = 0$. Having now arrived at our goal we write the Hamiltonian for a single atom as

$$H = \frac{1}{2}\begin{bmatrix} 0 & \Omega_{10}(t) & 0 \\ \Omega_{10}(t) & \Delta - \alpha_1 t & \Omega_{20}(t) \\ 0 & \Omega_{20}(t) & \delta - (\alpha_1 + \alpha_2)t \end{bmatrix}. \tag{12}$$

At this point we could use the above Hamiltonian to explore the population dynamics of a single atom in the field interaction representation. However, our next goal is to construct a collective spin Hamiltonian. In the next section, we will create such a Hamiltonian for a chain of three Rb atoms in a linear optical trap; we will refer to the diagonal elements of the single atom Hamiltonian in Equation (12) as

$$w_1 = 0, w_2 = \Delta - \alpha_1 t, w_3 = \delta - (\alpha_1 + \alpha_2)t. \tag{13}$$

III. The Collective Field-Interaction Hamiltonian for A Three-Atomic Chain

We apply the knowledge of the single atom Hamiltonian to create the Hamiltonian of a series of three interacting atoms trapped in a periodic, one-dimensional optical lattice and interacting via long-range interactions. These atoms are described by a model of three, three-level ladder subsystems interacting via the upper state, shown in Figure (2), by the van der Waals forces.

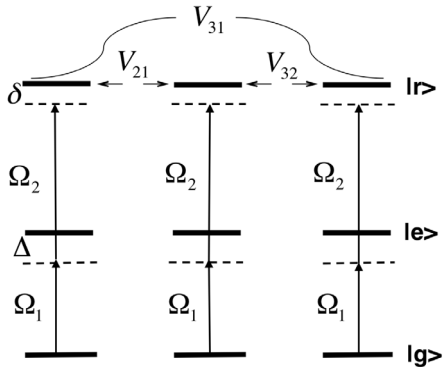

Figure 2: The scheme of a series of three interacting atoms.

Such system is represented by a wave function

$$|\psi(t)\rangle = \sum_{ijk}^{3N} A_{ijk}|ijk\rangle$$

in the basis of collective states $|ijk\rangle$, where i, j, and k represent the energy level of the first, the second and the third atom respectively. The dimension of the collective matrix Hamiltonian is 3N and is equal to 27 for the three-atomic configuration. Twelve different cases leading to non-zero off-diagonal matrix elements of the collective field-interaction Hamiltonian are present, but since the Hamiltonian is Hermitian, we only need to explain the six cases in the upper diagonals. These cases read as

$$\begin{aligned} \langle ij\mathbf{g}|\mathbf{e}ji\rangle &= \Omega_{10}(t) \\ \langle i\mathbf{g}k|k\mathbf{e}i\rangle &= \Omega_{10}(t) \\ \langle \mathbf{g}jk|kj\mathbf{e}\rangle &= \Omega_{10}(t) \\ \langle ij\mathbf{e}|\mathbf{r}ji\rangle &= \Omega_{20}(t) \\ \langle i\mathbf{e}k|k\mathbf{r}i\rangle &= \Omega_{20}(t) \\ \langle \mathbf{e}jk|kj\mathbf{r}\rangle &= \Omega_{20}(t). \end{aligned}$$

The diagonal matrix elements of this Hamiltonian are determined from Equation (12) and Equation (13) depending on what states are present in the respective basis function, e.g., for the $|reg\rangle$, the diagonal element is the bare state energy equal to $\omega_2 + \omega_3$ in the field interaction representation, (here, ω_1 would also be present, but it has a value of zero). There exist seven cases of degenerate states when two atoms are in the same substate, such as, e.g., $|rgg\rangle = |grg\rangle = |ggr\rangle$, all having energy ω_3 as shown in Figure (3). The exception to this is when two atoms are in the Rydberg state. Then an appropriate Rydberg-Rydberg interaction must also be accounted for, e.g., for the basis state $|rrg\rangle$ the diagonal matrix element is $2\omega_3 + 2V_{23}$. The coefficient of 2 in front of the Rydberg-Rydberg interaction comes as a result of the force on atom three from atom two, V_{23}, and vice versa. Since the Rydberg-Rydberg matrix is also Hermitian, $V_{23} = V_{32}$. The energy of state $|rgr\rangle$ is different though, and equal to $2\omega_3 + 2V_{13}$. Then, the truncated matrix of the collective field interaction Hamiltonian H may be written as

$$\begin{bmatrix} 0 & \Omega_1 & 0 & \dots & 0 & \dots & 0 \\ \Omega_1 & w_2 & \Omega_2 & \dots & 0 & \dots & 0 \\ 0 & \Omega_2 & w_3 & \dots & 0 & \dots & 0 \\ \vdots & \vdots & \vdots & \ddots & \vdots & \dots & 0 \\ 0 & 0 & 0 & \dots & 2w_3 + 2V_{23} & \dots & 0 \\ \vdots & \vdots & \vdots & \vdots & \vdots & \ddots & \vdots \\ 0 & 0 & 0 & 0 & 0 & \dots & 3w_3 + 2V_{max} \end{bmatrix} \tag{14}$$

Because of a degeneracy of certain states there are twelve unique energies dependent on the field parameters. They read as follows

$$
\begin{aligned}
E_1^{ggg}(t) &= 3\omega_1 \\
E_2^{geg,gge,egg}(t) &= 2\omega_1 + \omega_2 \\
E_3^{gee,eeg,ege}(t) &= \omega_1 + 2\omega_2 \\
E_4^{eee}(t) &= 3\omega_2 \\
E_5^{grg,rgg,ggr}(t) &= 2\omega_1 + \omega_3 \\
E_6^{ger,erg,rge,gre,egr,reg}(t) &= \omega_1 + \omega_2 + \omega_3 \\
E_7^{ere,eer,ree}(t) &= 2\omega_2 + \omega_3 \\
E_8^{grr,rrg}(t) &= \omega_1 + 2\omega_3 + 2V_{32} \\
E_9^{rgr}(t) &= \omega_1 + 2\omega_3 + 2V_{31} \\
E_{10}^{err,rre}(t) &= \omega_2 + 2\omega_3 + 2V_{32} \\
E_{11}^{rer}(t) &= \omega_2 + 2\omega_3 + 2V_{31} \\
E_{12}^{rrr}(t) &= 3\omega_3 + 2V_{max}.
\end{aligned}
\tag{15}
$$

Here $\omega_1 = 0$, $\omega_2 = \Delta - \alpha_1(t - t_c)$ and $\omega_3 = \delta - (\alpha_1 + \alpha_2)(t - t_c)$, and $V_{max} = V_{21} + V_{32} + V_{31}$.

IV. Dressed State Analysis as A Tool to Design the Control Scheme for A Generation of Multiparticle Coherent Superposition States

We refer to the dressed state picture aiming at the investigation of the dynamics of the collective spin states subject to the incident fields. Within the adiabatic approximation, we focus only one the first, the adiabatic term in the Schrödinger equation written in the dressed state basis

$$i\hbar\dot{\mathbf{C}}_\mathbf{d} = \mathbf{H_d C_d} - i\hbar\mathbf{T}\dot{\mathbf{T}}^\dagger\mathbf{C_d}. \tag{16}$$

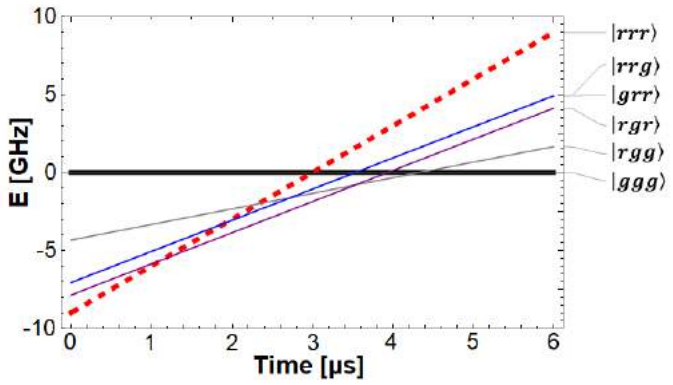

Figure 3: Energy of the relevant bare states in the field interaction representation as a function of time. Emphasized here are state $|ggg\rangle$ shown in black and state $|rrr\rangle$ shown in red dashes, these states are necessary for the formation of the GHZ state. States that contain ω_2 can be suppressed by manipulating the one photon detuning Δ and are not shown as they never interact with state $|ggg\rangle$.

Here $\mathbf{C_d} = \mathbf{TC}$ and $\mathbf{H_d} = \mathbf{T}^\dagger\,\mathbf{HT}$, $\mathbf{C_d}$ is the vector of the probability amplitudes of dressed states, $\mathbf{C}$ is that of the bare states in the field interaction representation, and $\mathbf{T}$ is the unitary transformation matrix. For example, for a two-level atomic system, which will be addressed later, and the unitary transformation matrix is $\mathbf{T(t)} = \mathbf{I}\cos\Theta(t) - i\boldsymbol{\sigma}_y\Theta(t)$, and

$$
\begin{aligned}
\cos\Theta(t) &= \left(1/2(1 + \delta(t)/\sqrt{\Omega_{eff}^2(t) + \delta^2(t)})\right)^{1/2} \\
\sin\Theta(t) &= \left(1/2(1 - \delta(t)/\sqrt{\Omega_{eff}^2(t) + \delta^2(t)})\right)^{1/2},
\end{aligned}
\tag{17}
$$

where $\Omega_{eff}(t)$ is the Rabi frequency, which couples the ground and the excited states. Our approach implies a variation of the field parameters to tune to a specific dynamics path by manipulating the desired avoided crossings of the energy of the bare states, which result in a predetermined superposition state by the end of pulse duration within adiabatic approximation. If there are more than one dressed state involved at the very end in order to have a desired superposition state, we conclude that non-adiabatic contribution cannot be neglected and overall, the dynamics is non-adiabatic. Because out of twelve energy-unique states only the ground state is field independent and is initially populated, any kind of population transfer is possible only through the avoided crossings.

According to the functional dependence of the energy of the states and aiming at achieving avoided crossings with the ground state, the following conditions have to be satisfied:

i) The one-photon and two-photon detuning Δ and δ must be negative in sign so that they give the starting negative values of the collective state energies;

ii) Chirp rates α_1 and α_2 have to be negative so that the energy slope is positive and the energies of all the states relevant for a creation of the GHZ and the W states will cross the zero energy of the initial state $|ggg\rangle$;

iii) The detuning must satisfy $|\Delta| \gg |\delta|$ so, that the transitional states dependent on Δ are significantly shifted and do not resonate with $|ggg\rangle$ during the pulse duration. This effectively means that any bare state containing an ω_2 parameter can be avoided while any state containing only ω_3 terms will cross and interact with the initial state $|ggg\rangle$.

To stir the population to a desired superposition state we use two, equally chirped pulses with $\alpha_1 = \alpha_2 = \alpha$ and completely overlapping Rabi frequencies $\Omega_1(t)$ and $\Omega_2(t)$ based on the control scheme developed for a deterministic excitation of a single atom to the Rydberg state [10]. To begin with, we analyse the qualitative behaviour of the bare states' energy depending on the choice of the field parameters. Figure (3) shows the time evolution of the energy of the collective bare states which depend on the two-photon detuning and the chirp rate and due to a proximity to the ground state energy (zero energy state) may contribute to the population dynamics.

The all-Rydberg state $|rrr\rangle$ inherently evolves the fastest due to three times doubled chirp rate in the energy $3(\delta\text{-}2\alpha(t\text{-}t_c))+2V_{max}$ which provides the leading crossing with the ground state. Thus, the desired avoided crossing is formed, which is the first within the pulse temporal evolution and the only one needed for the formation of the GHZ state. The time of the resonance, when two energy lines cross, is determined from the equality of the respective state's energy. Immediately after this resonance, the chirp must be turned off to prevent further approach of the lagging

transitional states to the zero-energy state to prevent undesirable population transfer.

The time of the crossing is equal to $t_{res} = (\delta/2+(V_{12}+V_{23}+V_{13})/3) / \alpha+t_c$. If $2(V_{12}+V_{23}+V_{13}) = 3\delta$, the resonance occurs at the same time as the peak intensity of the field t_c. Owing to the fact that the desired avoided crossing occurs the earliest in the time evolution implies that the intermediate state manifold, which consists of the rest 25 states for the three-atomic case, is not involved into a generation of the GHZ state and may be eliminated adiabatically within a semi-classical approach. Then adiabatic passage of a half of population to the all-Rydberg state is designed in the framework of an effective two-level system with the ground state being $|ggg\rangle$ and the excited state being $|rrr\rangle$. The effective Hamiltonian reads

$$\begin{aligned} \dot{a}_{ggg} &= i\Omega_{eff}(t)a_{rrr} \\ \dot{a}_{rrr} &= i6\alpha(t-t_c)a_{rrr} + i\Omega_{eff}(t)a_{ggg}, \end{aligned} \tag{18}$$

$$H_{eff}(t) = \hbar \begin{pmatrix} 0 & -\Omega_{eff}(t) \\ -\Omega_{eff}(t) & -6\alpha(t-t_c) \end{pmatrix}. \tag{19}$$

Here the effective Rabi frequency is $\Omega_{eff}(t) \sim \Omega_0{}^6/(\Delta^2 V^3)$. Within this two-level model, we design adiabatic passage leading to a coherent superposition of two states, $|ggg\rangle$ and $|rrr\rangle$, with equal populations. We rotate this Hamiltonian $H_{eff}(t)$ in Equation (19) using unitary transformation matrix **T** and bring it to the diagonal form $\hat{\mathbf{H}}_{\mathbf{d}}(t) = \mathbf{T}(t)\mathbf{H}_{\mathbf{eff}}(t)\mathbf{T}^{\dagger}(t)$. The $\hat{\mathbf{H}}_{\mathbf{d}}(t)$ is now written in the dressed state basis $\mathbf{C}_{\mathbf{d}}$. Aiming at creating the adiabatic passage condition, we assume adiabatic approximation with neglecting the second term in Equation (16).

Then, the adiabatic transition from $|ggg\rangle$ to $|rrr\rangle$ state takes place with in a single dressed state; this state has lower energy $E_I = -\hbar/2\sqrt{\Omega_{eff}^2 + \delta(t)^2}$ and reads

$$|\Psi(t)\rangle = e^{i\Lambda(t)/2}\left(\cos\Theta(t)|ggg\rangle - \sin\Theta(t)|rrr\rangle\right),$$

where $\Lambda(t) = \int_0^t \Omega(t')dt'$ is the pulse area. The details of the solution are presented in [11]. The coefficients are matrix elements of **T(t)**, which read as defined above in Equation (17). The control scheme to create the equal population distribution between states implies $\alpha \le 0$ for times $t \le t_c$ before the peak of the Gaussian pulse and $\alpha = 0$ for $t > t_c$ till the end of the pulse duration. At the initial time t=0, it provides the value of cos Θ (0) = 1 and sin Θ (0) = 0; meaning that the population is initially in the ground $|ggg\rangle$ state. Then at $t = t_c$, the probability amplitudes of two states change to become the same in magnitude: cos Θ $(t_c) = 1/\sqrt{2}$ and sin Θ $(t_c) = 1/\sqrt{2}$. At later times, $t > t_c$, the chirp is set to zero, and the field remains in the resonance with the transition frequency of the system till the end of the pulse duration, therefore any changes of the population are suppressed, (the applied field changes only the global dynamical phase), preserving the created superposition state. Thus, at the end of the pulse the probability amplitudes of $|ggg\rangle$ and $|rrr\rangle$ states are cos $\Theta(t_\infty) = 1/\sqrt{2}$ and sin $\Theta(t_\infty) = 1/\sqrt{2}$, giving the maximum state coherence.

However, in contrast to the case of the GHZ state, for the W state formation, the magnitude of the chirp parameter is preserved till the end of the pulse as it is required in order to allow all relevant, collective transitional states involved in forming the W state to populate by the end of the pulse. This can be observed in Figure (3), where state $|rrr\rangle$ cross $|ggg\rangle$ first, followed by states $|rrg\rangle$ and $|grr\rangle$ before finally $|rgr\rangle$ crosses. Among all collective states, we stir the evolution of states $|ggg\rangle$ and $|rrr\rangle$ relevant for the GHZ state and, alternatively, the evolution of the $|rrg\rangle$, $|grr\rangle$ $|rgr\rangle$ states relevant for the W state formation.

The entanglement fidelity function for the GHZ state is [12]

$$\begin{aligned} F_{GHZ} &= 1/\sqrt{2}(a_{rrr} + a_{ggg})^2 = \\ &1/2(a_{rrr}^2 + a_{ggg}^2 + a_{rrr}a_{ggg}^{\dagger} + a_{ggg}a_{rrr}^{\dagger}) \\ &1/2(a_{rrr}^2 + a_{ggg}^2 + 2Re\{a_{rrr}a_{ggg}^{\dagger}\}). \end{aligned} \tag{20}$$

For the W state, it reads

$$\begin{aligned} F_W &= 1/\sqrt{3}(a_{rrg} + a_{grr} + a_{rgr})^2 = \\ &1/3(a_{rrg}^2 + a_{grr}^2 + a_{rgr}^2 + a_{rrg}a_{grr}^{\dagger} \\ &+ a_{rrg}a_{rgr}^{\dagger} + a_{grr}a_{rrg}^{\dagger} + a_{grr}a_{rgr}^{\dagger} \\ &+ a_{rgr}a_{rrg}^{\dagger} + a_{rgr}a_{grr}^{\dagger}) = \\ &1/3(a_{rrg}^2 + a_{grr}^2 + a_{rgr}^2 + 2Re\{a_{rrg}a_{grr}^{\dagger}\} \\ &+ 2Re\{a_{rrg}a_{rgr}^{\dagger}\} + 2Re\{a_{grr}a_{rgr}^{\dagger}\}). \end{aligned} \tag{21}$$

The entanglement fidelity ranges from 1 to 0 and determines quantum correlations between the substates in the superposition.

V. Numerical Verification of the Quantum Control Schemes to Generate the Multipartite GHZ and the W States

We justify the developed quantum control methodology by applying it in a numerical exact solution of the time-dependent Schrödinger equation using the multiparticle field-interaction Hamiltonian in Equation (14) to generate the GHZ and the W state. The maximum fidelity of the GHZ state is achieved for the two-photon detuning $\delta = -2/3V_{max}$. However, the adiabatic approximation is not valid for the W state, because the dynamical process that stirs the three-atomic system to the required superposition state is inherently non-adiabatic with three dressed states participating at different stages of the pulse time evolution. Therefore, the maximum fidelity is found from the exact solution of the time dependent Schrödinger equation, which accounts for the non-adiabatic effects.

The exact solution of the time-dependent Schrödinger equation was performed numerically using the Runge-Kutta method and a numerical method based on multipoint Hermit interpolating polynomials [13, 14]. In calculations to generate the GHZ state the following values of the parameters of the fields were used: the pulse duration is $\tau_0 = 1\mu s$, the one-photon detuning is Δ= -1.5 GHz, and the peak Rabi frequency of both applied pulses is $\Omega_{01(2)}$, it changes in the range from 0 to 300 MHz, the chirp rate is $\alpha_{1,2}$, it changes in the range from 0 to -600 MHz / μs, and the two-photon detuning is $\delta = -2/3V_{max}$, which has two values, δ = -100MHz for V_{31} =V/2 and δ = -80.63MHz for V_{31} = V/2[6]

for nearest neighbour interaction equal to V = 60MHz. Numerical analysis demonstrates the generation of the GHZ state via two-photon adiabatic passage with the same chirp rate $\alpha_{1,2} = \alpha$ of two pulses and the same overlapping Rabi frequencies $\Omega_{01(2)}(t)$.

The fidelity of the GHZ state is shown in Figure (4a) and Figure (4c) as a function of the chirp rate and the strength of the peak Rabi frequency for $V_{31} = V/2$ (a) and $V_{31} = V/2^6$ (c). The optimal values of the fidelity within 0.995 range are highlighted by the contour plots. Figure (4b) and Figure (4d) show the density plot of the difference between the populations of the $|ggg\rangle$ and the $|rrr\rangle$ states and brings an additional information for a complete picture of the GHZ state formation. The zero values of the population difference indicate upon equal populations of these states, while fidelity about 0.995 in the same region of the field parameters carries information about high phase correlation between atoms. A comparison of the results for $V_{31} = V/2$ (a), (b) and $V_{31} = V/2^6$ (c), (d) suggests that for the generation the GHZ state with high fidelity, a wider choice of the field parameters is possible for a smaller value of the interaction between terminal atoms V_{31}. For $V_{31} = V/2^6$, the results are more robust for experimental realization, but at the expense of a higher field amplitude.

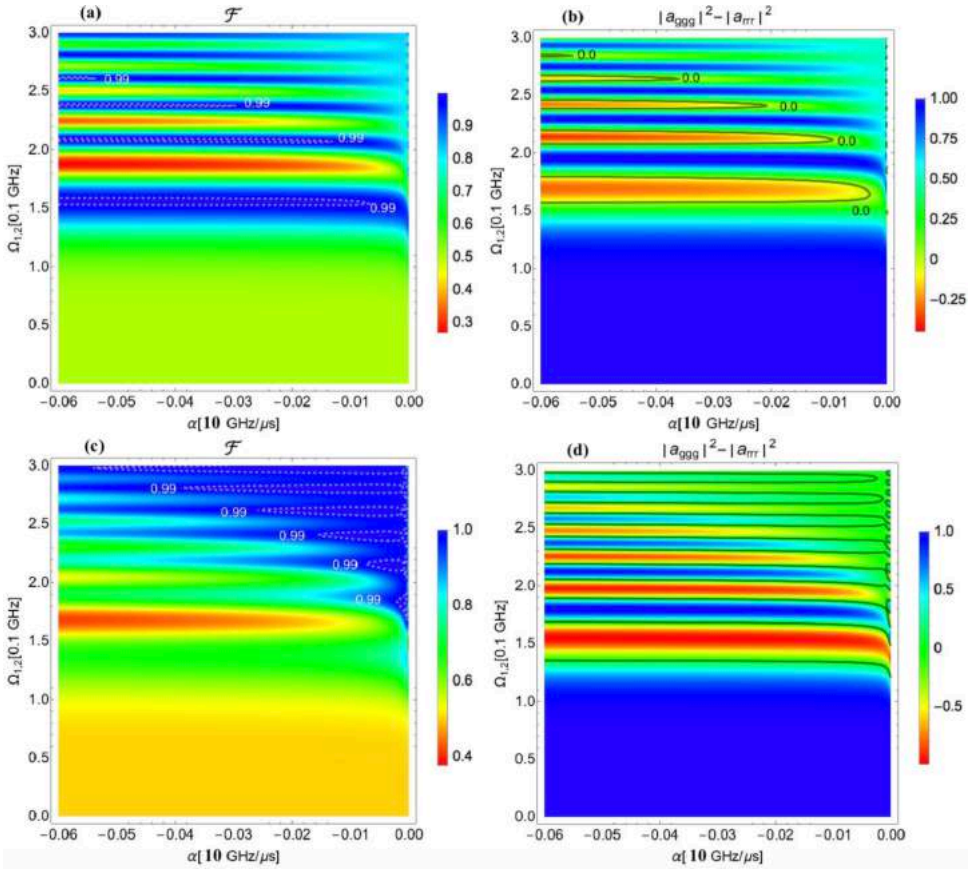

Figure 4: (a) Fidelity of the GHZ state as a function of the chirp rate and the peak Rabi frequency for $V_{31} = V/2$, V_{max} = 150MHz; (b) The population difference of states $|ggg\rangle$ and $|rrr\rangle$ as a function of the chirp rate and the peak Rabi frequency for $V_{31} = V/2$, V_{max} = 150MHz. (c) Fidelity of the GHZ state as a function of the chirp rate and the peak Rabi frequency for $V_{31} = V/2^6$, V_{max} = 120.94 MHz; (d) The population difference of states $|ggg\rangle$ and $|rrr\rangle$ as a function of the chirp rate and the peak Rabi frequency for $V_{31} = V/2^6$, V_{max} = 120.94MHz. Parameters used in calculation are V = 60MHz, τ_0 = 1μs, Δ = -1.5GHz, and $\delta = -2/3V_{max}$.

The time dependence of the population of the $|ggg\rangle$ and $|rrr\rangle$ states leading to the formation of the GHZ state at the end of the pulse duration is shown in Figure (5) demonstrating adiabatic passage for parameters of the field Δ = -1.5GHz, δ = -100MHz, $\Omega_{01(2)}$ = 158MHz, α = -176MHz/μs, and V_{max} = 150MHz.

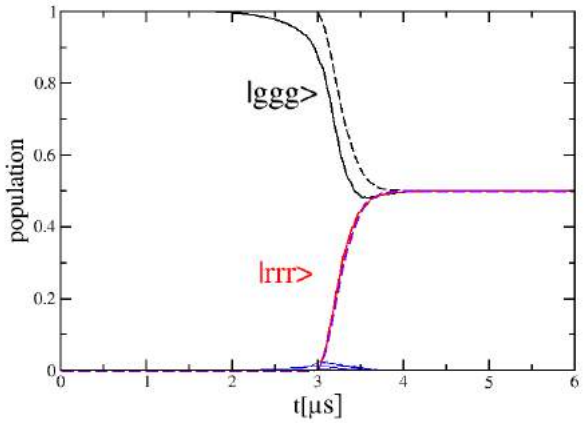

Figure 5: The time dependence of the population of the $|ggg\rangle$ and $|rrr\rangle$ states leading to the formation of the GHZ state at the end of the pulse duration for parameters of the field τ_0 = 1μs, Δ= -1.5GHz, δ= -100MHz, $\Omega_{01(2)}$ = 158MHz, α = -176MHz/μs, and V_{max} = 150MHz. Dashed curves show an approximate solution using Eqs (18).

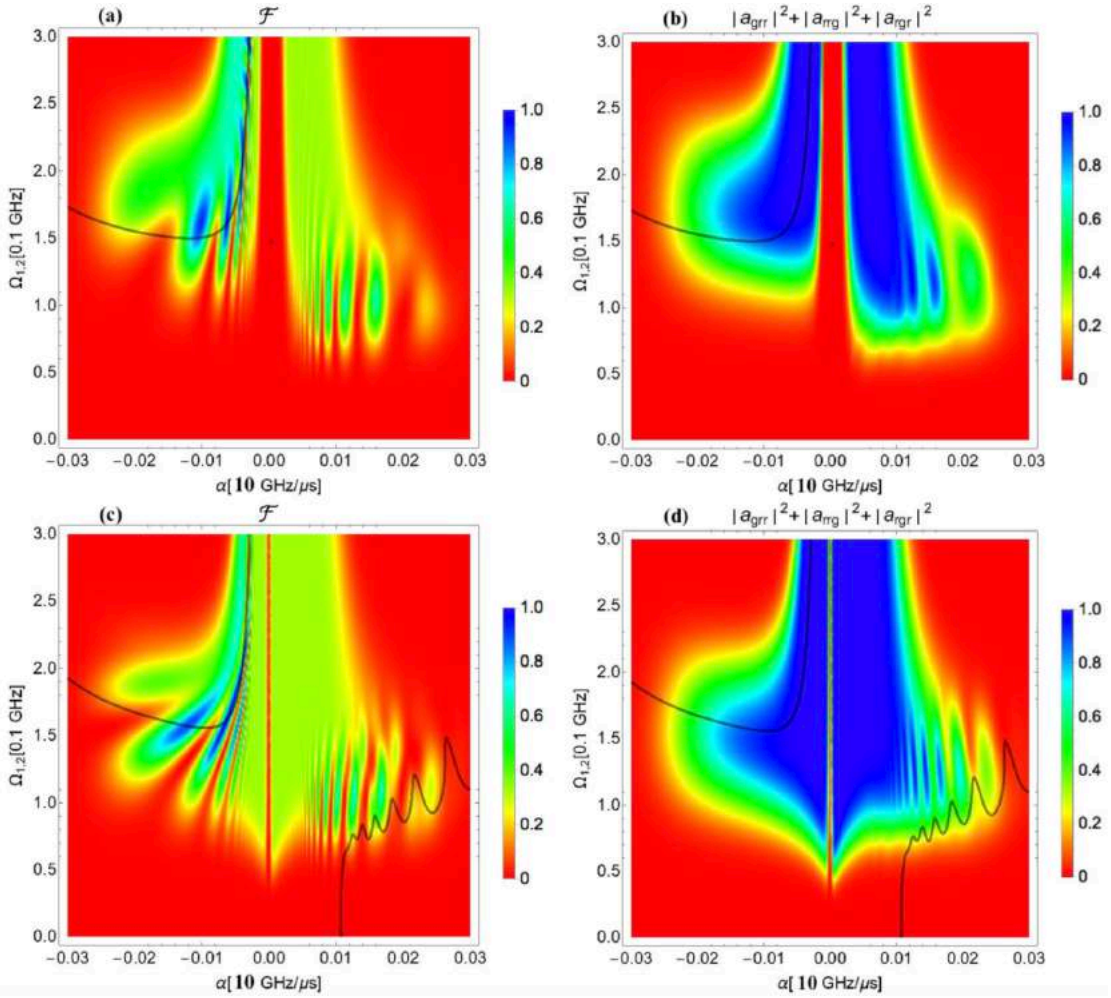

Figure 6: (a) Fidelity of the W state as a function of the chirp rate and the peak Rabi frequency for V_{31} = V/2, V_{max} = 150MHz; (b) The density plot of the sum of populations of $|rrg\rangle$, $|grr\rangle$ and $|rgr\rangle$ states for V_{31} = V/2, V_{max} = 150MHz. (c) Fidelity of the W state as a function of the chirp rate and the peak Rabi frequency for V_{31} = V/2^6; V_{max} = 120.94MHz; (d) The density plot of the sum of populations of $|rrg\rangle$, $|grr\rangle$ and $|rgr\rangle$ states for V_{31}=V/2^6 , V_{max} = 120.94MHz. Parameters used in calculation are V = 60MHz, τ_0 = 1μs, Δ = -1.4GHz, and δ = -4.5MHz. The black curves draw the contour where three contributing states have equal population.

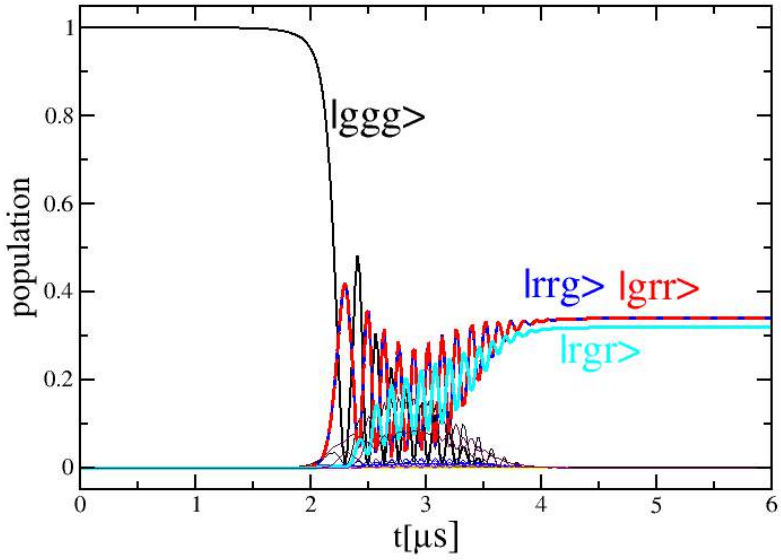

Figure 7: Time dependence of population of the $|grr\rangle$, $|rrg\rangle$ and $|rgr\rangle$ states leading to the formation of the W state at the end of the pulse duration for parameters of the field τ_0 = 1μs, Δ=-1.4 GHz, δ=-4.5 MHz, $\Omega_{01(2)}$ =262 MHz, α=-32 MHz/μs, and $V_{21} = V_{32} = 2V_{31} = V$ =60MHz.

In numerical calculations of the W state generation the following values of the parameters of the fields were used: The pulse duration is τ_0 = 1μs, the chirp rate is $\alpha_{1,2}$, it varies in the range from 0 to -300MHz/μs, the two-photon detuning is δ = -4.5MHz, the one-photon detuning is Δ = -1.4GHz, and the peak Rabi frequency of both applied pulses is $\Omega_{01(2)}$, it varies in the range from 0 to 300MHz. Two values of the parameter V_{31} were used, $V_{31} = V/2$ and $V_{31} = V/2^6$, which provide V_{max} = 150MHz and V_{max} = 120.94MHz respectively, for nearest neighbour interaction equal to V = 60MHz.

Figure (6a) and Figure (6c) show fidelity of the W state as a function of the chirp rate and the peak Rabi frequency for $V_{31} = V/2$ (a) and $V_{31} = V/2^6$ (c). Strong dependence on $\alpha_{1,2}$ and $\Omega_{01(2)}$ is observed indicating upon nonadiabatic regime of light-matter interaction. The black curve draws the contour where three contributing states have equal population. The blue regions of fidelity through which this curve passes manifest highest values owing to equal population of the contributing states and the same phase between them. Figure (6b) and Figure (6d) show the density plots of the sum of populations of $|rrg\rangle$, $|grr\rangle$ and $|rgr\rangle$ states for $V_{31} = V/2$ (b) and $V_{31} = V/2^6$ (d). Together with the density plots of the difference of populations between $|rrg\rangle$ and $|rgr\rangle$, (not shown here), they provided sufficient information to draw the contours of equal populations.

By comparing the results for $V_{31} = V/2$ (a), (b) and $V_{31} = V/2^6$ (c), (d) we conclude that a smaller value of the interaction between terminal atoms somewhat improves the results for the generation the W state, meaning that the target area of the field parameters providing higher fidelity states is increased. However, since the process of the W state generation is principally non-adiabatic with at least three dressed states populated, the considered change in the value of V_{31} does not substantially change the non-adiabatic coupling between the important dressed states, (one of which correlates with $|ggg\rangle$ state at t=0, while another correlate with $|grr\rangle$, $|rrg\rangle$ and $|rgr\rangle$ at final time.)

The dynamics of the population of the $|rrg\rangle$, $|grr\rangle$ and $|rgr\rangle$ states, forming the W state is shown in Figure (7) for Δ=-1.4 GHz, δ=-4.5MHz, $\Omega_{01(2)}$ =262 MHz, α=-32 MHz/μs, and $V_{21} = V_{32} = 2V_{31} = V$ =60MHz. The Rabi oscillations between the mostly populated states $|rrg\rangle$, $|grr\rangle$ and $|rgr\rangle$ are clearly shown at the intermediate times. These oscillations can be explained by the non-adiabatic coupling between states in the dressed state picture indicating upon the non-adiabatic nature of the W state formation. The fidelity of such state formation is 0.999 and is among the highest values in the provided numerical results. Parameters used in the time dependent calculations of Figure (5) and Figure (7) may be used to explore the experimental realizations of the GHZ and W states.

The lifetime of the Rydberg states is on the order of 100μs, while the pulse duration used in our method is 1μs. Two orders of magnitude difference permit us to neglect the decoherence effects in the systems during control operations with the applied fields. Besides, one-photon detuning from intermediate state of 1.5 GHz is about an order of magnitude larger than the natural bandwidth of these states known to be ~10 ns [15, 16]. Such detuning results in a negligible population of transitional states minimizing decoherence. In principle, a one-photon excitation, which would need a photon in the ultraviolet range [17], may be used to excite atoms to a predetermined magnetic sublevel of the Rydberg state. However, the two-photon excitation scheme is more robust because it requires visible light; it is commonly used in Rydberg experiments with trapped alkali atoms. Besides, it offers a broader range of control parameters including the one-photon and the two-photon detuning, which bring flexibility to the control scheme to perform adiabatic passage on large atomic systems. Strong Rydberg-Rydberg interactions provide significant collective energy shifts beneficial for controllable excitations of predetermined collective states. Meanwhile, a long lifetime of Rydberg states is efficient for quantum operations.

VI. Conclusion

Quantum control of multiparticle entangled states generation involving coherent superpositions of spin states in ultracold Rydberg atoms is presented based on the two-photon passage on the selected state manifold using circularly polarized and linearly chirped pulses. Selectivity of states is achieved through the choice of the one-photon and the two-photon detuning, the ratio of the Rabi frequency to the collective coupling strength and the chirp rate. It is shown that the creation of the GHZ sate is adiabatic passage in nature, while the W entangled state generation is inherently non-adiabatic process. These results are of fundamental interest and usefulness aiming at a controlled generation of the entangled states in large ensembles of trapped atoms.

Acknowledgment

Authors acknowledge support from the Office of Naval Research.

References

1. Greenberger, D. M., Horne, M. A., Shimony, A., & Zeilinger, A. (1990). Bell's theorem without inequalities. American Journal of Physics, 58(12), 1131-1143.
2. Dür. W. (2001). Multipartite entanglement that is robust against disposal of particles. Phys. Rev. A 63, 020303.
3. Briegel, H. J., Raussendorf, R. (2001). Persistent Entanglement in Arrays of Interacting Particles. Phys. Rev. Lett. 86, 910.
4. Dür, W., Vidal, G., and Cirac. J. I. (2000). Three qubits can be entangled in two inequivalent ways. Phys Rev. A 62, 062314.
5. Xia, Y., Fu, C. B., Zhang, S., Hong, S. K., Yeon, K. H., & Um, C. I. (2006). Quantum dialogue by using the GHZ state. arXiv preprint quant-ph/0601127.
6. Hai-Jing, C., Song. H. (2006). Quantum Secure Direct Communication with W State. Chin. Phys. Lett. 23, 290.
7. Omran, A., Levine, H., Keesling, A., Semeghini, G., Wang, T. T., Ebadi, S., ... & Lukin, M. D. (2019). Generation and manipulation of Schrödinger cat states in Rydberg atom arrays. Science, 365(6453), 570-574.
8. Zhang, C. L., Wang, C., Cao, C., & Zhang, R. (2012). Multi-particle entanglement generation using quantum-dot spin and optical microcavity system. Chinese Physics Letters, 29(7), 070305.
9. Kang, Y. H., Chen, Y. H., Wu, Q. C., Huang, B. H., Song, J., & Xia, Y. (2016). Fast generation of W states of superconducting qubits with multiple Schrödinger dynamics. Scientific reports, 6(1), 1-13.
10. Kuznetsova, E., Liu, G., & Malinovskaya, S. A. (2014). Adiabatic rapid passage two-photon excitation of a Rydberg atom. Physica Scripta, 2014(T160), 014024.
11. Ramaswamy, A., Malinovskaya, S. A., in preparation (2023).
12. Pachniak, E., & Malinovskaya, S. A. (2021). Creation of quantum entangled states of Rydberg atoms via chirped adiabatic passage. Scientific Reports, 11(1), 1-9.
13. Press, W.H., Teukolsky, S.A., Vetterling, W.T., Flannery, B.P. (2001). Numerical Recipes in Fortran 77. Cambridge University Press, Cambridge.
14. Latypov, A. F., & Nikulichev, Y. V. (2007). Numerical methods based on multipoint Hermite interpolating polynomials for solving the Cauchy problem for stiff systems of ordinary differential equations. Computational Mathematics and Mathematical Physics, 47(2), 227-237.
15. Gallagher, T. F. (2005). Rydberg Atoms Cambridge Univ.
16. Feichtner, J. D., Gallagher, J. H., & Mizushima, M. (1967). Lifetime of the First Excited Atomic States of Rb 87. Physical Review, 164(1), 44.
17. Beterov, I. I., Tretyakov, D. B., Entin, V. M., Yakshina, E. A., Ryabtsev, I. I., MacCormick, C., & Bergamini, S. (2011). Deterministic single-atom excitation via adiabatic passage and Rydberg blockade. Physical Review A, 84(2), 023413.